Effect of Microstructure on Notch Fatigue Properties of Ti-6Al-4V

D. EYLON AND C. M. PIERCE

The effect of microstructure on the notch fatigue properties of Ti-6Al-4V was investigated. Specimens with five distinctly different microstructures were tested and subsequently examined in detail. It was found that the notch fatigue performance of the alloy varied significantly as the microstructure was altered by heat treatment. The best high cycle fatigue strength was found in specimens heat treated above the beta transus temperature, containing an almost totally transformed acicular alpha structure. The fatigue performance of specimens with this microstructure appeared to be controlled by the size of the nucleated crack. It is suggested that at low stress levels the nucleated crack is limited in size to the width of a single alpha needle, while at high stresses the nucleated crack may be as large as an entire colony of similarly aligned alpha needles.

IT is generally held that the smooth fatigue behavior of alloys is more sensitive to changes in microstructure than notched fatigue.[1] The reason given for this observation is the fact that during the initiation stage of the fatigue crack, the plastic zone at the front of the crack in a smooth specimen is smaller than that in a notched specimen and therefore more sensitive to microstructural features. Since, in titanium alloys, it is possible to obtain many different microstructures in a single alloy through differing combinations of processing and heat treating (Hall *et al*),[2] the smooth fatigue behavior of titanium should be very much dependent on the prior history of the material. The fact that processing and heat treating can control the smooth fatigue behavior of titanium through changes in microstructure, has indeed been shown by Bowen and Stubbington,[3,4,5] by Lucas,[6,7] and by Margolin, *et al*.[8]

In addition, extensive examination of the fatigue behavior of components and joints in airframes by Crichlow[9,10] showed that, unlike steels or aluminum alloys, titanium alloys showed significant scatter in their fatigue behavior. In fact the scatter for the titanium alloys is almost two times greater than that of aluminum alloys and three times greater than that of steels. This proportion was found to be approximately the same for both constant amplitude and spectrum loading test conditions. These observations on components were supported by test data on notched coupons and the same conclusion was reached in work done by Whittaker.[11,12]

The purpose of this investigation was to determine the degree to which microstructural modifications affect the notch fatigue properties of the most commonly used titanium alloy in airframe construction, Ti-6Al-4V. Microstructural variations in actual practice can be due not only to differing processing/heat treatment procedures, but also due to section size effects in a single component. Bowen and Stubbington,[3] for example, showed that specimens from different locations in a large Ti-6Al-4V section gave differing smooth fatigue strengths because of microstructural and textural variations. If the notch fatigue strength is also as dependent on the microstructural conditions, then these observations could explain in some part the large scatter in fatigue results on titanium components and joints.

Although the tests in this investigation were conducted on laboratory size specimens, special effort was made to simulate the microstructural conditions commonly observed in actual components. Five microstructures commonly obtained through differing heat treatments on a two inch thick plate were synthesized in thinner laboratory specimens by appropriate modifications of the heat treatment parameters. These modifications were also designed to give the test coupons approximately the same tensile strength and to therefore lead to a more appropriate evaluation of the fatigue data. To elucidate several important interrelationships, the fatigue crack growth rate and the fracture toughness of specimens having the same five microstructural conditions were also examined.

EXPERIMENTAL PROCEDURE

A. Material

All material tested in this investigation was taken from a single Ti-6Al-4V 2 × 10 × 79 in. (50 × 250 × 2000 mm) plate, cross rolled at 1750°F (954°C) and mill annealed. The final rolling direction was identified, and all tensile, fatigue, fracture toughness, and fatigue crack growth rate specimens were machined so that the tensile axis was in the rolling direction and the crack propagation path was in the width direction of the rolled plate (*LT* crack plane orientation—ASTM designation E399.72). The composition of the alloy plate is given in Table I.

B. Heat Treatment

Five heat treatment procedures, yielding five different microstructural conditions, were selected. These heat treatment procedures are listed in Table II. Prior to heat treatment, the material was cut into test coupons, slightly larger than the final machined specimen size. The coupons were heat treated in an air furnace

D. EYLON was a National Research Council Associate at the Air Force Materials Laboratory and is now with the Department of Materials Science and Metallurgical Engineering at the University of Cincinnati, Cincinnati, Ohio 45221. C. M. PIERCE is with the Air Force Materials Laboratory, Wright-Patterson Air Force Base, Ohio 45433.

Manuscript submitted February 5, 1975.

Table I. The Chemical Composition of the Ti-6Al-4V Alloy

Element	Wt Pct
C	0.018
Fe	0.16
N	0.014
Al	6.3
V	4.3
H	0.005
O	0.16

Table II. Heat Treatment Conditions

Heat Treatment Group	Heat Treatment Conditions
A	As received (mill annealed)
B	1700°F (927°C)/4 h (at temp). Furnace cool to 1400°F (760°C). Air cool to room temperature.
C	1750°F (954°C)/2 h (at temp). Water quench to room temperature. 1400°F (760°C)/4 h (at temp). Air cool to room temperature.
D	1750°F (954°C)/2 h (at temp), 1500°F (816°C)/1 h (at temp). Air cool to room temperature.
E	1900°F (1038°C)/1 h (at temp). Air cool to room temperature. 1350°F (732°C)/4 h (at temp). Air cool to room temperature.

with a temperature control accuracy of ± 5°F (3°C). The oxygen contamination found in the heat treated coupons was checked by the microhardness method used by Reynolds, Ogden and Jaffee.[13] For all heat treatments the oxygen penetration never exceeded 0.5 mm. Therefore the removal of at least 2 mm of material from each side of the coupon during final specimen machining assured that the oxygen content in the test specimens was close to the as received value (Table I). Based on a previous investigation,[14] involving the heat treatment of the 2 in. thick (50 mm) thick plate itself, it was known that the five microstructural conditions were also obtainable by conventional heat treatment methods.

C. Tensile Tests

Tensile testing was performed at room temperature on a 10 ton capacity Instron machine at a crosshead speed of 0.008 in. (0.2 mm) per min. Tensile specimens were machined according to ASTM E8.69 specifications for small size round specimens, with 0.16 in. (4.1 mm) diameter and 0.64 in. (16.3 mm) gage length.

D. Fatigue Tests

Fatigue testing was performed on a 6 ton axial loading Schenck fatigue machine at 2000 rpm. The loading wave form was sinusoidal and all tests were done at a stress ratio of $R = 0.1$. The specimen geometry was that of the flat centernotched type, shown in Fig. 1(*a*). As stated previously, the specimens were machined from the heat treated coupons, so that almost equal amounts of material were removed from each side of the coupons, in order to avoid oxygen contamination. The center notch itself was made by drilling three holes as shown in Fig. 1(*b*), resulting in a stress concentration factor for this hole geometry[15] of $K_t = 3.5$. The surfaces of the specimens were ground to an RMS

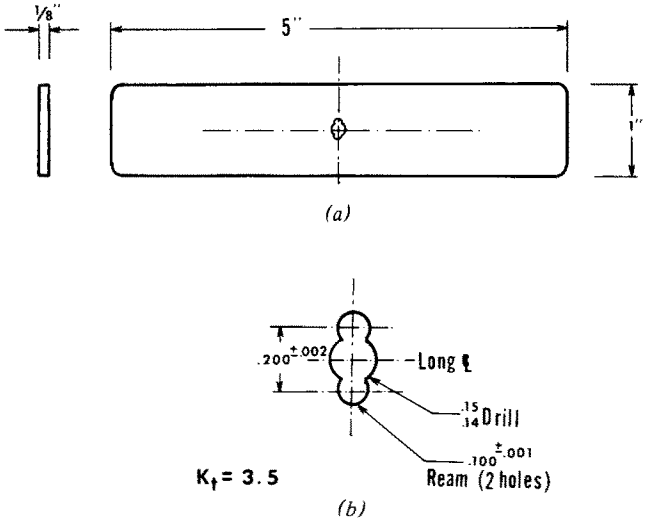

Fig. 1—Flat notch fatigue specimen, (*a*) general view, (*b*) notch detail. All dimensions are given in inches.

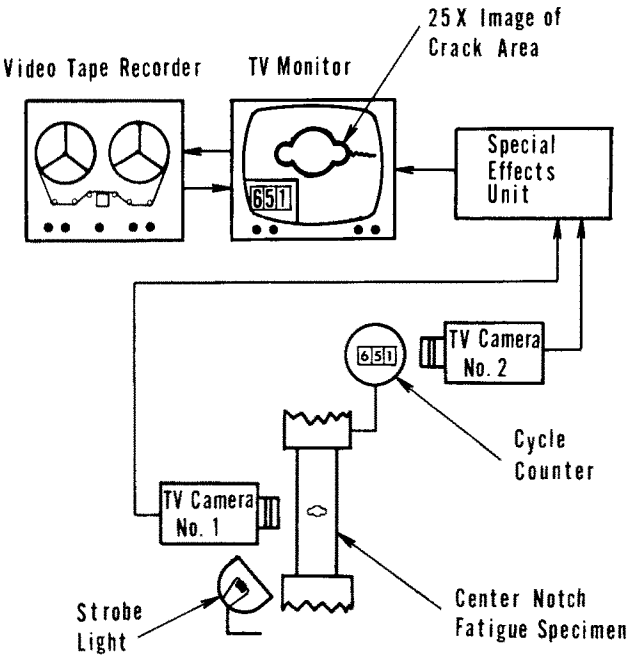

Fig. 2—Closed circuit television recording system, for the determination of the number of cycles for crack initiation.

16 finish and the center holes were reamed after drilling.

In order to determine some measure of the number of fatigue cycles required for an arbitrary crack initiation size, the fatigue testing rig was equipped with the special closed circuit television recording system described in Fig. 2. While one TV camera gave a magnified (25X) picture of the center notch zone with an accuracy of 0.1 mm, the second camera was focused on the fatigue cycle counter. Both pictures were monitored on the same TV screen by a special effects unit and were continuously recorded on slow motion video tape recorder. To properly illuminate the center notch area, a stroboscopic high intensity flash light was synchronized with the machine frequency. Through this method it was possible to detect an initial crack approximately 0.5 mm in length. After frac-

ture of a fatigue specimen, the video tape recording was replayed to determine the number of cycles required for initiation of a 0.5 mm crack. By using the double TV camera system, one can also conduct a rapid fatigue crack growth rate test, since the replay procedure can give the number of cycles corresponding to any crack length. It should be noted that the TV crack detection system cannot provide the same resolution as can an optical system with the same magnification due to the loss of resolution in the video recording and on the monitor screen. In this system it was possible to detect crack length increments in the order of 0.2 mm. This method is only adequate to get a quick rough estimate of the number of cycles to a given crack length. To obtain more accurate fatigue crack growth rate data, compact tension specimens were used in this work.

E. Fracture Toughness Tests

Fracture toughness tests were performed on a 0.75 in. (19.1 mm) compact tensile specimen according to ASTM designation E399.72. The precracking of the specimens was done on an MTS 811.02 machine, and the pull test on a 10 ton capacity Instron machine at a cross head speed of 0.1 in. (2.5 mm) per min. Fracture surface examination after specimens were pulled to failure indicated that in each case the crack front profile satisfied E399.72 requirements. All results listed as K_{IC} values satisfied the ASTM requirements for a valid plane strain fracture toughness test. Several did not satisfy the thickness requirement and are designated as K_Q.

F. Fatigue Crack Growth Rate Tests

Fatigue crack growth rate tests were performed on a 0.75 in. (19.1 mm) thick compact tensile specimen, machined in accordance with ASTM designation E399.72. The tests were done on an MTS 811.02 machine, using a sinusoidal load wave form of 10 Hz at a stress ratio of $R = 0.1$. The crack length was measured with a 30X traveling microscope. Crack length measurements were performed on both sides of the specimens and averaged for both growth increments and stress intensity calculations. The stress intensity range ΔK was defined as:

$$\Delta K = K_{\max} - K_{\min} = \frac{P_{\max} - P_{\min}}{BW^{1/2}} f\left(\frac{a}{W}\right) \qquad [1]$$

where $K_{\max}$ is the stress intensity factor at the maximum load ($P_{\max}$) point of the cycle, $K_{\min}$ is the stress intensity factor at the minimum load ($P_{\min}$) point of the cycle, B is the thickness and W is the depth of the specimen. Both a = the crack length and $f(a/W)$ are defined and calculated according to E399.72.

G. Texture Examination

The texture was determined by an X-ray reflection pole figure of the basal plane (0002) using a Norelco diffractometer. The specimens were hand polished and etched to remove any surface material containing residual stresses.

H. Metallographic Examination

Metallographic examination was performed on electro-polished surfaces using a Kroll etch. In general the microstructures shown in this work will be represented by their image on the LT plane (L-rolling, T-long transverse and S-short transverse directions). The isometric microstructural figures were prepared by also using photomicrographs from the LS and TS planes. Since up to six specimens could be machined from the 2 inch thick plate, considerable attention was paid to the microstructural uniformity of coupons cut from different locations through the thickness of the plate.

I. Fractographic Examination

Optical fractographic examinations of tested fatigue specimens, representing all five microstructures, were performed normal to the fracture surface on the LT plane. In several fatigue specimens the initiation site of the crack could be positively identified. Some of these specimens polished down to the plane of the crack origin. This way the initiation site could be identified in the microstructure. The fracture face itself was examined with scanning electron microscopy. Optical metallographic examinations of the fatigue crack growth rate specimens normal to the fracture surface were also performed.

RESULTS

A. Microstructure

The microstructures which resulted from the five heat treatments employed in this investigation (Table II) are presented in Figs. 3 through 7. The as received

Fig. 3—*A* type microstructure. As received (mill annealed). Magnification 445 times.

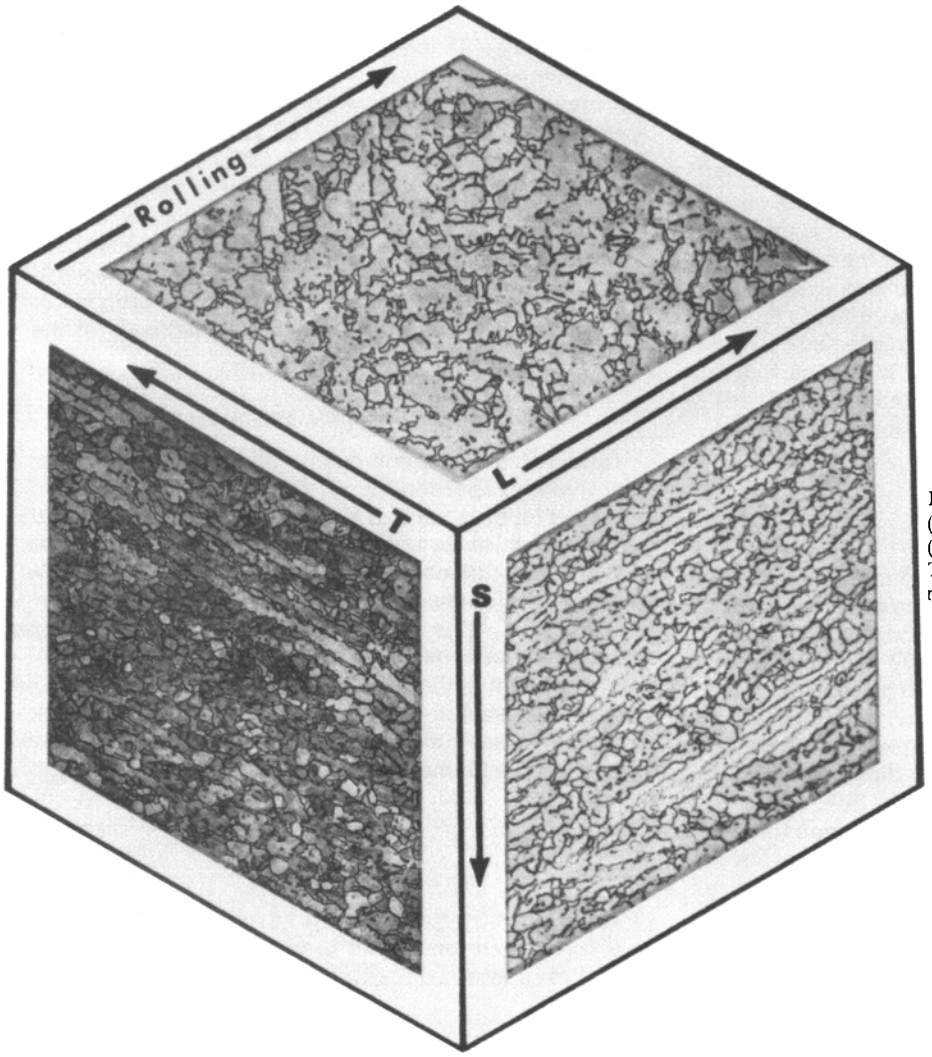

Fig. 4—*B* type microstructure. 1700°F (927°C)/4 h, furnace cooled to 1400°F (760°C), air cooled to room temperature. Three dimensional microstructure. Magnification 150 times.

(condition *A*) microstructure (Fig. 3) contained large elongated alpha plates (about 80 vol pct) separated by islands of beta or finely transformed beta. The microstructure which resulted from furnace cooling from an alpha-beta solution heat treatment temperature (condition *B*) (Fig. 4), contained large globular alpha particles (about 70 vol pct) in a beta or a finely transformed beta matrix. Fig. 5 shows a microstructure with small globular alpha particles (about 50 vol pct) and fine acicular alpha in a beta or finely transformed beta matrix. This microstructure (condition *C*) resulted from solution heat treating the alloy in the alpha-beta region, water quenching and overaging. Fig. 6 also shows small globular alpha phase particles but with coarse acicular alpha in a beta or finely transformed beta matrix. The coarse acicular alpha structure (condition *D*) was obtained by interrupted cooling from a solution treatment temperature. This type of microstructure is commonly found in larger sections which have been air cooled from the solution treatment temperature. Fig. 7 shows the almost totally transformed acicular alpha structure (condition *E*) associated with material solution heat treated above the beta transus. Fig. 14(*b*) shows the same microstructure, at higher magnification.

B. Microstructural Homogeneity

All microstructures, with the exception of *E* (Fig. 7), showed very strong alpha grain directionality in both the *TS* and *LS* planes due to the cross rolling. Figs. 4 and 7 are three dimensional representations of the *B* and of the *E* type microstructures, respectively. Solution heat treatment above the beta transus temperature seemed to "erase" all the directionality effects of the prior processing and resulted in an acicular alpha phase microstructure with almost equiaxed prior beta grains structure. Microstructures of specimens similarly heat treated but taken from different locations through the thickness of the large plate were also examined. Fig. 6 is an example of the uniform microstructure pattern found in this type of examination. In this case the *D* type microstructure is shown. Only the as received material (*A*-type microstructure) showed a slightly different microstructure upon examination of the plate surface (location 3 in Fig. 6), and therefore test specimens were not machined from that area.

C. Texture

The crystallographic textures associated with the five microstructural conditions are represented by the

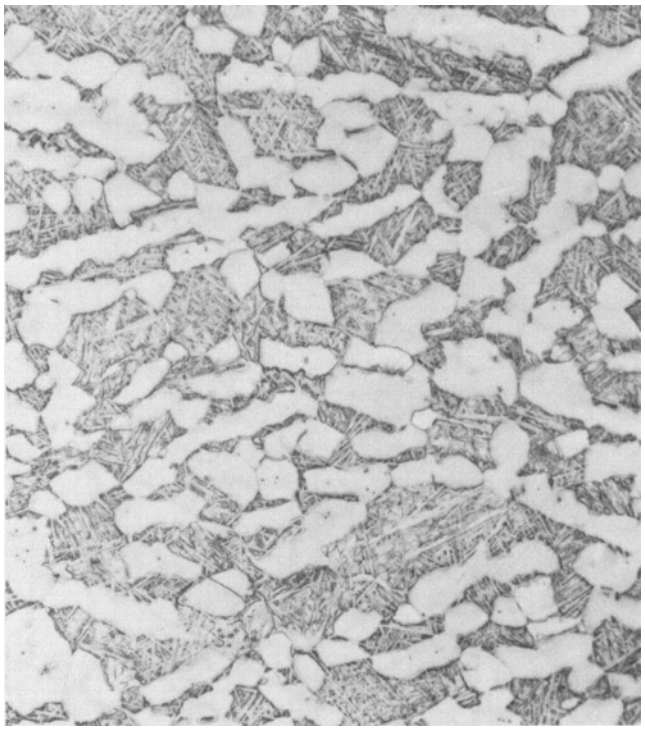

Fig. 5—*C* type microstructure. 1750°F (954°C)/2 h, water quenched, 1400°F (760°C)/4 h, air cooled to room temperature. Magnification 445 times.

(0002) pole figures in Fig. 8. The *L* direction represents the last rolling direction of the cross rolled plate. Only that material heat treated in the beta phase region (Fig. 8(*e*)) contained basal planes which were nearly parallel to the rolling plane.

D. Tensile Properties

The tensile properties obtained are listed in Table III. Three specimens from each microstructural group were tested. The listed values are the resultant average. It should be noted that the maximum deviation in average tensile strength for all five microstructural conditions is only 18.6 MN/mm^2 (2.7 ksi); however, material receiving treatment *E* exhibited a much lower ductility relative to the other values.

E. Fatigue Properties

Fig. 9 shows the *S-N* fatigue curve for the as-received material (Type *A*). Each data point represents a single specimen value, and this curve was selected to be shown individually because it exhibited the largest scatter observed in the testing of the five microstructural groups. Fig. 10 shows the *S-N* curve for microstructural type *B*, which exhibited the smallest data point scatter. The degrees of scatter in the *S-N* curves associated with the other three microstructural types (*C*, *D*, *E*) were far closer in their nature to that in Fig. 10 than in that shown in Fig. 9. Fig. 11 shows the *S-N* fatigue curves for all five microstructural types. Since it was very unusual, it should be noted that those type *E* specimens which were tested in the high cycle fatigue portion of the curve failed close to the grips instead of at the center notch area. In spite of this fact, microstructural condition *E* exhibited the best high cycle fatigue strength.

F. Fatigue Crack Initiation

By using the two camera close circuit television recording system, the number of cycles to initiation of a 0.5 mm crack and the number of cycles to fracture were recorded. By simple subtraction it was then possible to calculate the number of cycles required for propagation of the crack from 0.5 mm to final fracture. Fig. 12 shows the percent of fatigue life which was spent in propagating the crack over this range *vs* the total fatigue life of each specimen.

G. Fatigue Crack Growth Rate

Fig. 13 shows the measured fatigue crack growth rate (da/dN) for the five different microstructures as a function of the stress intensity range (ΔK). The ΔK range in this figure is purposely extended in order to better distinguish any differences in behavior due to microstructural condition. Each curve in Fig. 13 represents the results obtained on a single specimen.

H. Fracture Toughness

The plane strain fracture toughness (K_{IC}) results for the five different microstructural groups are presented in Table IV. The values shown are the average of two tests from each group. Since only 0.75 in. (19.1 mm) thick compact tension specimens were used, the results obtained on the *E* type microstructure could not satisfy the requirement for a valid test of:

$$B \geq 2.5\left(\frac{K_{IC}}{\sigma_{ys}}\right) \qquad [2]$$

where B is the thickness of the specimen, and σ_{ys} is the yield strength. Therefore these results are listed in Table IV as K_Q values.

I. Fractographic Examination

Optical examination of the fatigue specimens normal to the fracture surface indicated that the crack path was relatively straight and perpendicular to the tensile axis for material in conditions *A-D*.

Fig. 14(*a*) represents this typical crack growth behavior in specimen of condition *A*. On the other hand the crack path in specimens of condition *E* (Fig. 14(*b*)) was far more jagged in appearance. For reasons that will be discussed, the microstructure at the initiation sites of condition *E* fatigue specimens was investigated. Those tested at the higher stress levels, showed straight fracture line at the initiation site (Fig. 14(*b*)). The size and the angle of this initial fracture suggest that it may be a result of a shear through one or more colonies of alpha needles. The fatigue specimens tested at the lower stress levels, showed only short initial fracture about the size of the width of a single alpha needle.

Scanning electron microscopy of the fracture surfaces of fatigue specimens also showed a significant difference between specimens of condition *E* and those in the other conditions. Figs. 15(*a*) and (*b*), which were taken within 0.5 mm from the notch initiation site, il-

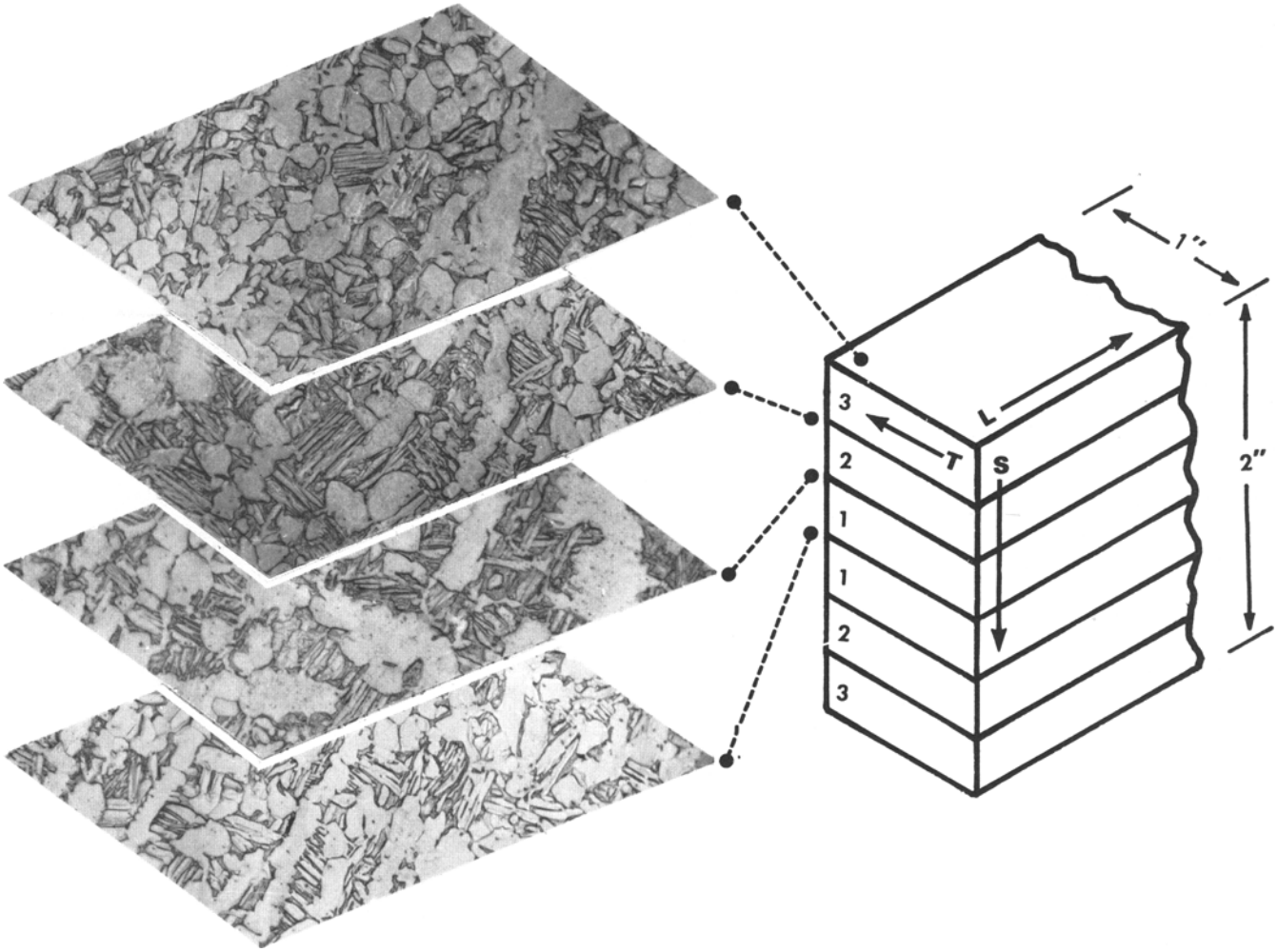

Fig. 6—*D* type microstructure. 1750°F (954°C)/2 h, 1500°F (816°C)/1 h, air cooled to room temperature. Microstructures of specimens taken from 4 different locations across the thickness (*S* direction) of the 2 in. Ti-6Al-4V plate, magnification 328 times.

lustrate this point. Fig. 15(*b*) (condition *E*) indicates that crack branching normal to the principal crack direction occurred extensively. Upon examining many fatigue specimens of condition *E* at difference distances from the notch it was found that this tendency for branch cracking was most prevalent near the initiation site of highly stressed specimens.

DISCUSSION

The effect of microstructural features on the notch fatigue properties of Ti-6Al-4V is shown in Fig. 11. In the high stress region, little difference was noted between the five conditions; however, at low stresses, condition *E* exhibited superior life, conditions *C*, *B*, and *D* were quite similar and intermediate in performance, while condition *A* had the lowest observed values. In order to understand these results, it is necessary to consider the individual events which occur prior to specimen failure. Fig. 16 is a schematic of the crack path indicating the position of the crack at first nucleation (A_n), the experimental observation of initiation (A_i), which was 0.5 mm, and the critical crack size at unstable fracture (A_c).

The total life in cycles (N_t) can be expressed in a simplified manner as the sum of the number of cycles to the observed initiated crack length of 0.5 mm (N_i), and (N_p) the number of cycles for stable crack growth between A_i and A_c:

$$N_t = N_i + N_p \qquad [3]$$

Although there is a great deal of scatter (particularly for specimens of condition *E*), the plot shown in Fig. 12 indicates that N_p can be neglected compared to N_i in the low stress/high cycle regime. The number of cycles to observed initiation (N_i) is a function of the number of cycles to first crack nucleation (N_n), the size of the nucleated crack (A_n), and the crack growth rate from A_n to A_i.

In Table V the ΔK values for the centernotched fatigue specimens with 0.5 mm length of crack were calculated similarly to the calculation of the ΔK of the fatigue crack growth rate specimens. In the low stress range of the fatigue testing, the calculated ΔK values were always less than 30 $MN/M^{3/2}$. Although the fatigue crack growth rates shown in Fig. 13 were obtained on thicker specimens than those used in the fatigue test, the data indicates that at ΔK values less than 30 $MN/M^{3/2}$, the crack growth rates for all five microstructural conditions are identical. The differences noted in fatigue behavior in the low stress range

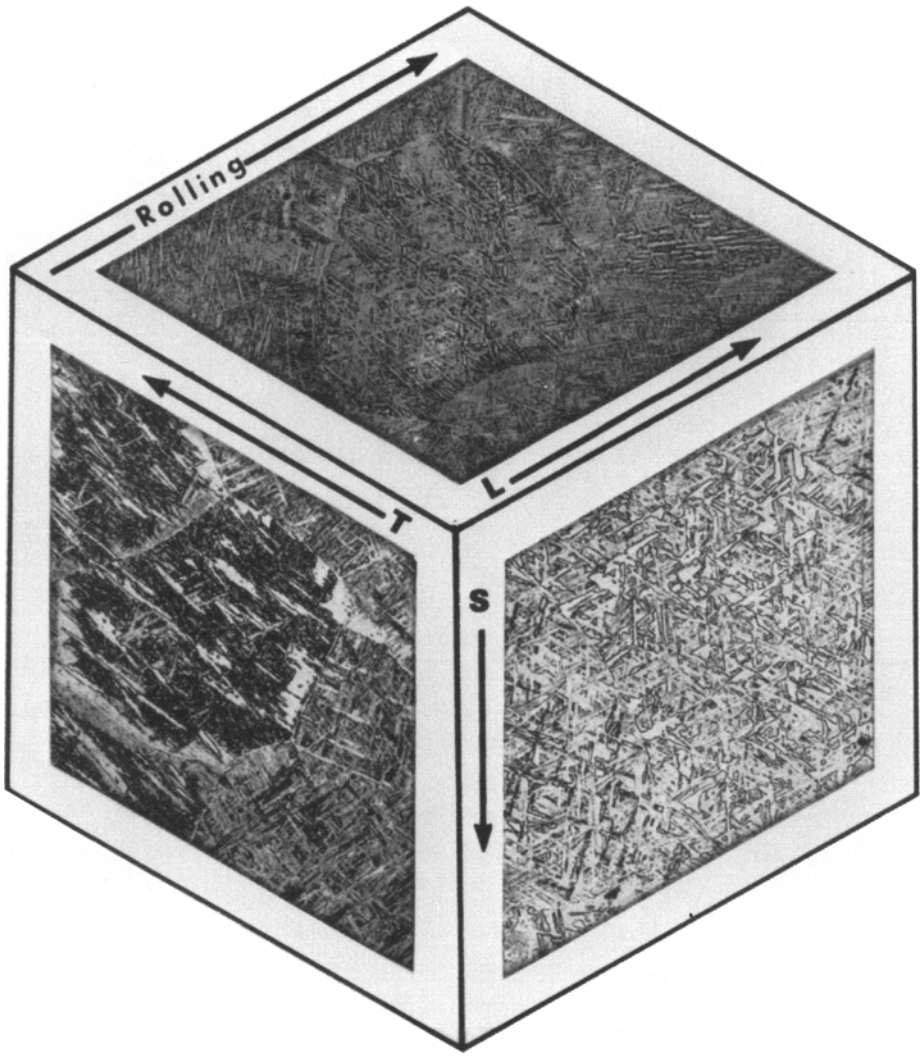

Fig. 7—*E* type microstructure. 1900°F (1038°C)/1 h, air cooled to room temperature. 1350°F (732°C)/4 h, air cooled to room temperature. Three dimensional microstructure. Magnification 150 times.

can therefore only be related to the nucleation event, specifically either to the number of cycles to crack nucleation (N_n) or to the length of the nucleated crack (A_n). The authors can therefore suggest two explanations for the higher fatigue strength of specimens in condition *E*.

It is possible that the number of cycles to nucleate a crack (N_n) was greater for this material due to its significantly different texture (see Fig. 8). Several investigators have identified texture as being an important factor in fatigue performance of titanium alloys.[16,17,18] Although the microstructure of condition *E* was very dissimilar from that used by Zarkades and Larson,[19] their results indicated that the texture associated with condition *E* can improve the fatigue performance of Ti-6Al-4V. The effect of texture on the fatigue performance of titanium alloys should be explored in more detail since uncertainties concerning its role do not allow the authors to positively define the microstructural influences.

It is possible, however, that at low stress levels the size of the nucleated crack (A_n) is limited to the width of the alpha needles, which is considerably smaller than the size of the alpha grains associated with conditions *A* through *D*. The alpha grain size may well represent the limiting size of nucleated cracks in two phase microstructures (*A-D*). Fatigue tests of the Ti-6Al-4V[5] and IMI-685 titanium alloys,[20] and fatigue crack growth rate specimens of the Ti-11 titanium alloy[21] have shown that in the transformed beta acicular structure cracks do prefer to nucleate in the width direction of acicular alpha needles, along a shear band on the basal plane. Since this type of mechanism would be expected to be dependent on the state-of-stress, it offers an explanation for the fact, previously noted, that the low stress fatigue specimens of condition *E* failed close to the grips instead of at the center notch area. The area immediately adjacent to the grips is subjected to a complex state of stress as a result of the compressive force of the grips.

Since the suggested mechanism based on a limited length of nucleated crack (A_n) is supported by direct observation of preferred crack nucleation sites by several investigators in Ti-6Al-4V[5] and similar alloys,[20,21] and, as will be discussed later, offers a rationale for the high stress behavior, the authors tend to favor this latter explanation.

The lower fatigue strength of the as-received specimens (condition *A*) is thought to be due to the effect of residual stresses inherent in the starting 2 in. (50 mm) plate material. All other conditions (*B-E*) provide for a reheat treatment after machining to coupon dimen-

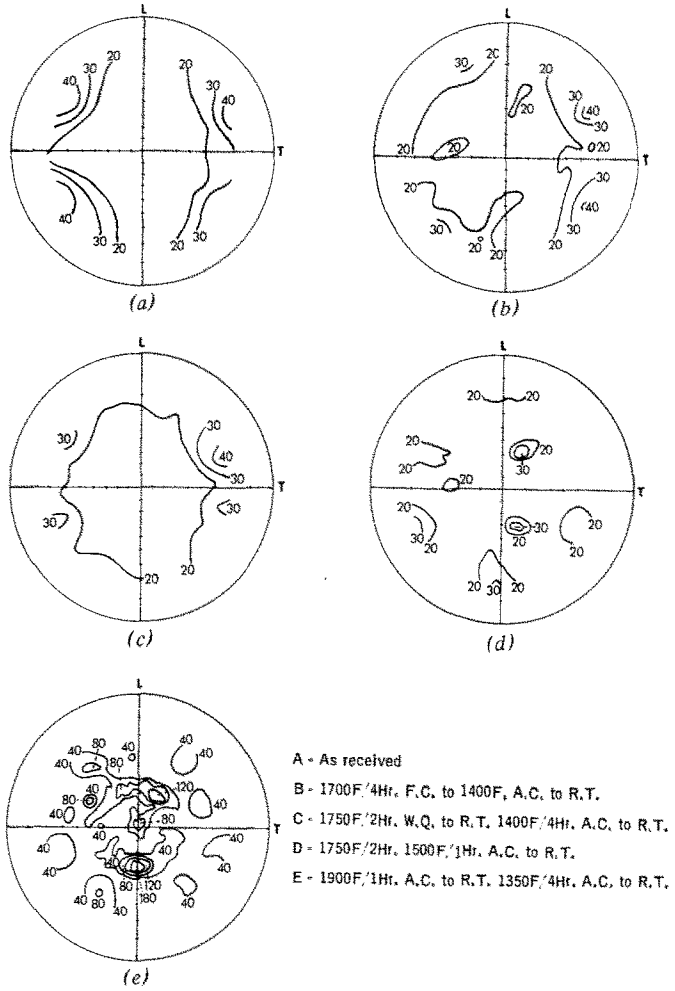

Fig. 8—(0002) pole figures of: (*a*) *A* condition, (*b*) *B* condition, (*c*) *C* condition, (*d*) *D* condition, (*e*) *E* condition. *L* is the last rolling direction of the 2 in. (50 mm) thick plate.

Table III. Tensile Properties of the Different Heat Treatment Conditions, in the Rolling Direction (*L* Direction)

Heat Treatment	*Y.S.* (0.2 pct) MN/m^2	*T.S.*, MN/m^2	Elongation, Pct	*R.A.*, Pct
A	880	952	12.7	36.2
B	843	961	13.7	35.4
C	896	978	17.0	38.3
D	887	985	14.2	42.2
E	860	956	8.8	21.5

Specimen Dimensions: $D_0 = 0.16$ in. (4.1 mm), $L_0 = 0.65$ in. (16.5 mm)
Strain Rate = 0.008 in./in. per min.

sions. The larger scatter of data points in Fig. 9, especially at the low stress range of the curve, can be interpreted as supporting evidence for this suggestion.

When considering the high stress/low cycle region of the fatigue curve, the data in Fig. 12 suggests that the number of cycles for propagation (N_p) in Eq. [3] can no longer be neglected. N_p is a function of the fracture toughness (which determines A_c) and the crack growth rate at moderately high levels of ΔK. Table V shows that ΔK values of 30 $MN/m^{3/2}$ and above must now be considered.

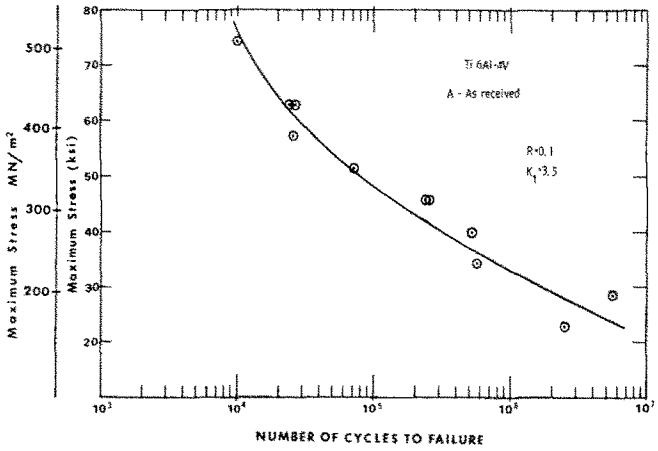

Fig. 9—*S-N* fatigue curve for fatigue specimens in condition *A* (as received).

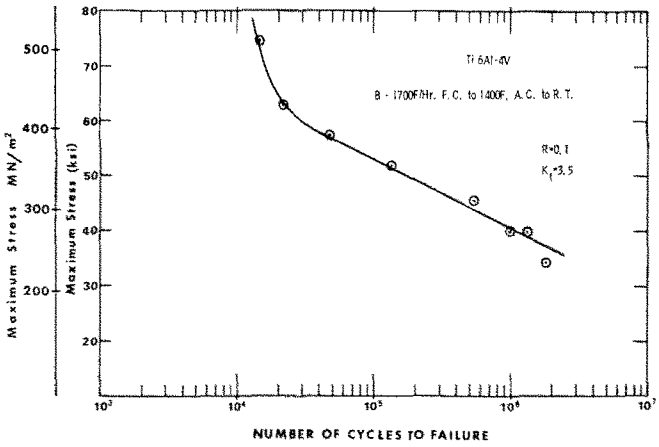

Fig. 10—*S-N* fatigue curve for fatigue specimens in condition *B*.

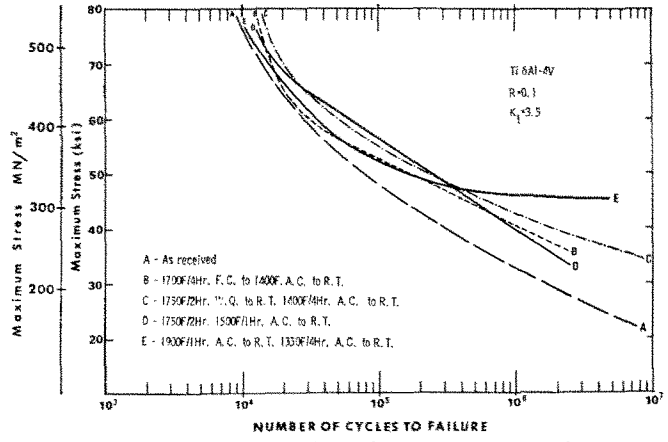

Fig. 11—*S-N* fatigue curves for all 5 microstructural conditions.

It is of interest to note that both the fatigue crack growth rate (see Fig. 13) and the fracture toughness (see Table IV) of the condition *E* material are superior to all others. Nevertheless, as noted earlier, there is little difference in the fatigue life of the various microstructural conditions in this high stress range. Therefore, in the case of condition *E*, N_i must be unusually low to compensate for the aforementioned higher value in N_p. In addition, from previous discus-

sion, the crack growth rate from A_n to A_i is approximately the same for all conditions. This lower value of N_i in the high stress regime must now be attributed to the nucleation event, which was previously described as consisting of either the number of cycles to crack nucleation (N_n) or to the length of the nucleated crack (A_n).

The author's attribute this behavior, however, to the large A_n which can be seen in Fig. 14(*b*) in the acicular structure at the high stress levels. One of the possible explanations offered earlier in an attempt to explain an excellent fatigue behavior of the *E* type microstructure at low stress levels involved the preferential nucleation of cracks in the width direction of acicular needles. Eylon, Hall, and Pierce[20,21] and Shechtman and Roberson[22] showed that at high stress levels a shear band can proceed through colonies of similarly aligned acicular alpha plates unhindered from one needle to another in a single occurrence. This mechanism may be responsible for nucleating a crack as large as one or more colonies of alpha needles (see Fig. 14(*b*)). This proposed mechanism provides an explanation for the stress dependence noticed in the fatigue behavior of the *E* type microstructure.

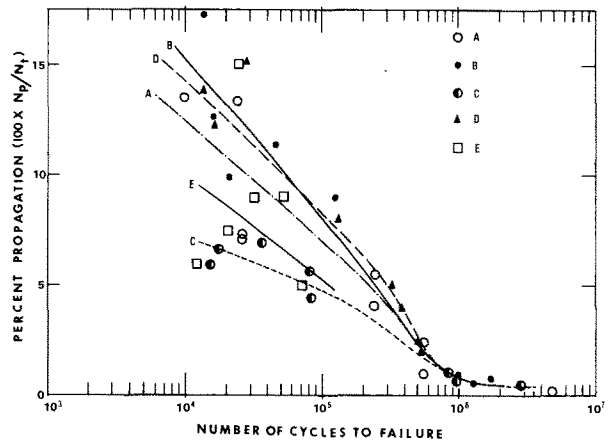

Fig. 12—Percent of fatigue life which was spent in propagating the crack from 0.5 mm to fracture, *vs* number of cycles to failure, for all 5 microstructural conditions.

CONCLUSIONS

1) The microstructural conditions obtained in Ti-

Table IV. The K_{IC} and the K_Q Values for All Five Microstructural Conditions

	Group				
	A	*B*	*C*	*D*	*E*
K_{IC}, MN/m$^{3/2}$	49.7	55.7	53.9	60.0	
K_Q, MN/m$^{3/2}$					83.8

Table V. The ΔK Values of the Centernotched Fatigue Specimens with 0.5 mm Crack at Different Maximum Stress Levels

Maximum Stress, MN/m^2	ΔK for 0.5 mm Crack, MN/m$^{3/2}$
512.3	40.1
473.0	37.2
433.7	34.0
393.7	30.9
354.4	27.8
315.1	24.8
275.8	21.7
236.5	18.6
197.2	15.5

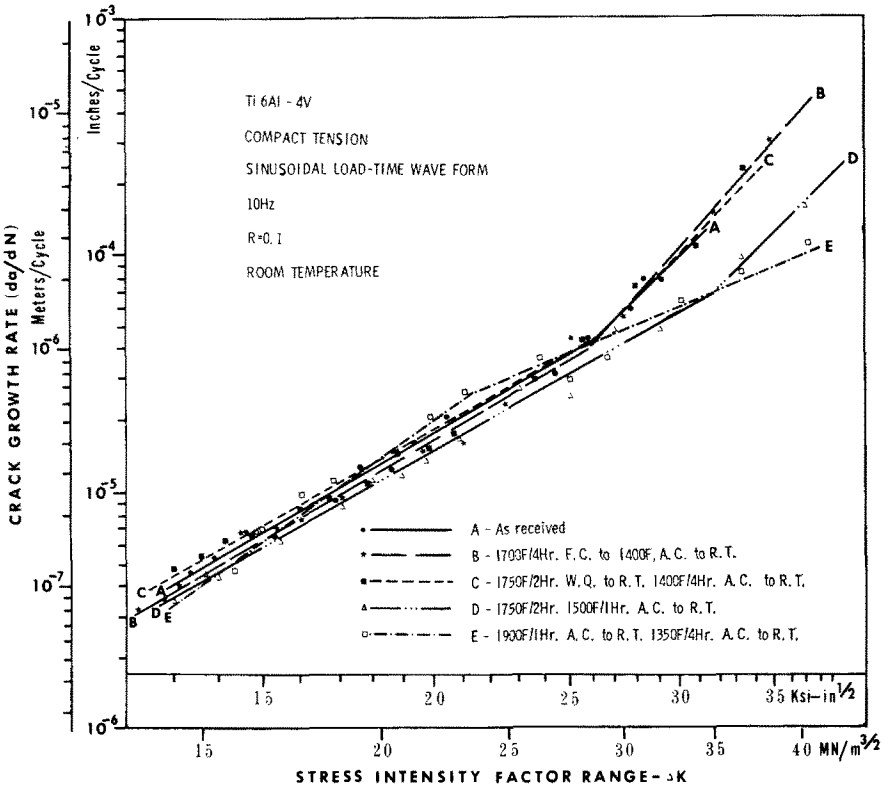

Fig. 13—Fatigue crack growth rates (da/dN) for all 5 microstructural conditions, as a function of the stress intensity range (ΔK).

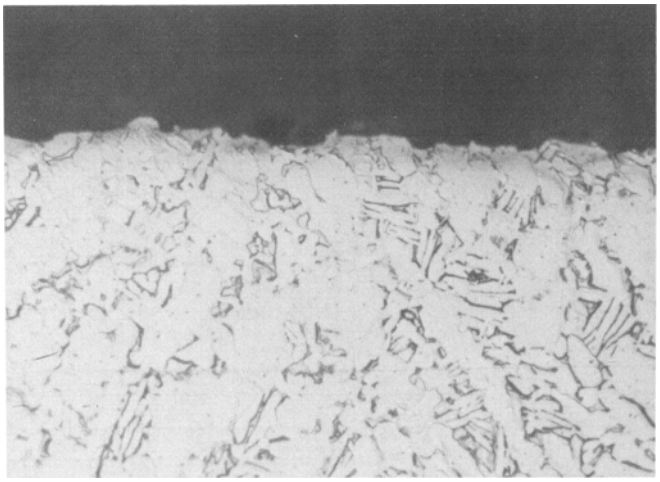

(a)

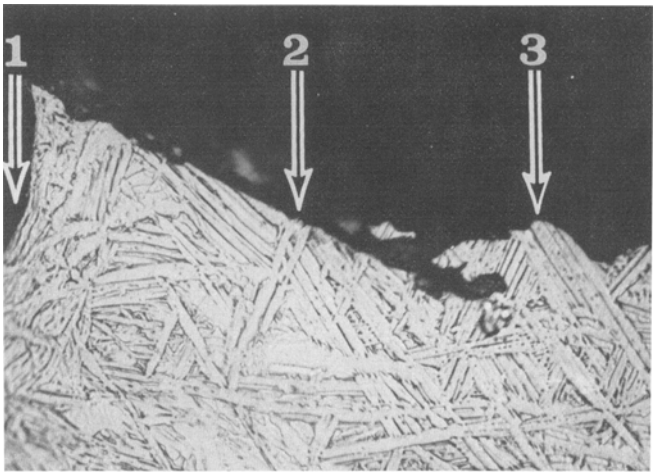

(b)

Fig. 14—Micrographs taken normal to the fatigue fracture surface of (*a*) condition *A*. Maximum stress 433.3 MN/mm^2 (62.9 KSI). Magnification 340 times. (*b*) condition *E*. Maximum stress 472.7 MN/mm^2 (68.6 KSI). Magnification 780 times. 1. Center notch. 2. Nucleated crack. 3. Fatigue propagation.

6Al-4V significantly affect the notched fatigue performance of the alloy.

2) The best high cycle fatigue strength for the alloy was found in specimens heat treated above the beta transus containing an almost totally transformed acicular alpha structure.

3) The size of the nucleated crack in the transformed acicular alpha structure appears to control its fatigue performance. This parameter, however, is very stress dependent. At low stress, the nucleated crack is limited to the width of an individual alpha needle; while at high stresses, the nucleated crack can be as large as one or more colonies of similarly aligned alpha needles. This latter fact detracts significantly from the relatively lower crack growth rate (at high ΔK values) and the high K_{IC} values associated with this microstructure.

ACKNOWLEDGMENTS

The authors wish to thank David E. Kirk of Monsanto Research Corporation, Dayton, Ohio, for the

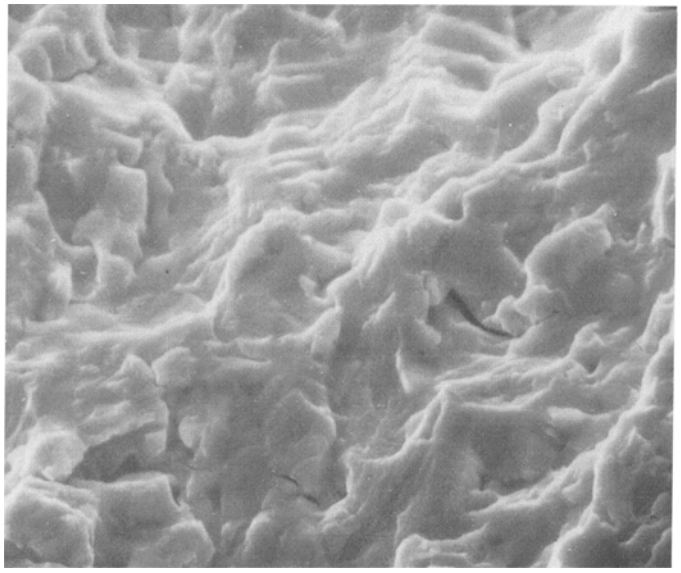

(a)

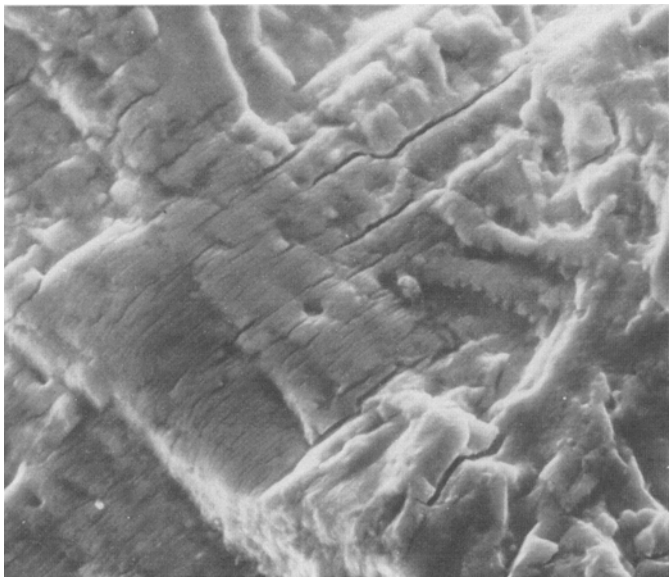

(b)

Fig. 15—SEM fractographs taken from the fatigue fracture surface of (*a*) condition *A*, initiation. Maximum stress 511.9 MN/mm^2 (74.3 KSI). Magnification 1000 times. (*b*) condition *E*, initiation. Maximum stress 472.7 MN/mm^2 (68.6 KSI). Magnification 1000 times. Pictures (*a*) and (*b*) were taken within 0.5 mm from the notch initiation site.

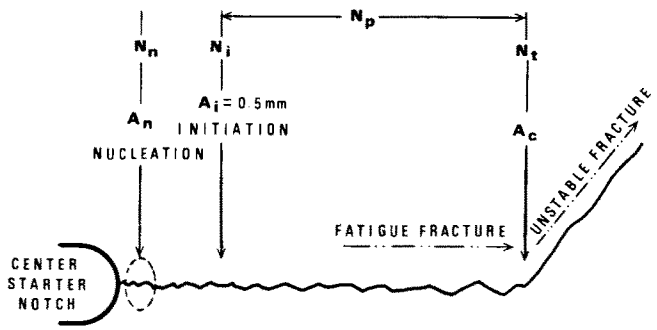

Fig. 16—A schematic of the crack path in flat center notch fatigue specimen.

excellent conduction of most of the experiments in this work.

REFERENCES

1. A. M. Freudenthal: *Eng. Fract. Mech.*, 1973, vol. 5, pp. 403-14.
2. J. A. Hall, C. M. Pierce, D. L. Ruckle, and R. A. Sprague: *Mater. Sci. Eng.*, 1972, vol. 9, pp. 197-210.
3. A. W. Bowen and C. A. Stubbington: *Titanium Science and Technology*, vol. 3, pp. 2097-108, Plenum Press, New York, 1973.
4. C. A. Stubbington and A. W. Bowen: *Titanium Science and Technology*, vol. 2, pp. 1288-96, Plenum Press, New York, 1973.
5. C. A. Stubbington and A. W. Bowen: *RAE Tech. Report 73036*, Royal Aircraft Establishment, Farnborough, England, May 1973.
6. J. J. Lucas: *Titanium Science and Technology*, vol. 3, pp. 2081-95, Plenum Press, New York, 1973.
7. J. J. Lucas and P. P. Konieczny: *Met. Trans.*, 1971, vol. 2, pp. 911-12.
8. H. Margolin, S. Patel, and Y. Mahajan: Final report on Contract Nr. N00024-72-C-5465, Naval Ship Systems Command, January 1974.
9. W. J. Crichlow: *Titanium Science and Technology*, vol. 2, pp. 1257-70, Plenum Press, New York, 1973.
10. W. J. Crichlow: AGARD Lecture Series No. 62 on "Fatigue Life Prediction for Aircraft Structures and Materials," Munich, Paris, and Ottawa, June 1973.
11. I. C. Whittaker: *Report No. AFML-TR-72-236*, Air Force Materials Laboratory, October 1972.
12. I. C. Whittaker and I. C. Beanner: *Report No. AFML-TR-69-65*, Air Force Materials Laboratory, April 1969.
13. J. E. Reynolds, H. R. Ogden, and R. I. Jaffee: *Trans. ASM*, 1957, vol. 49, pp. 280-99.
14. P. L. Hendricks: *AIAA/ASME/SAE 15th Structures, Structural Dynamics and Materials Conference*, Las Vegas, Nev., April 1974, Paper No. 74-374.
15. *ASTM STP 91, Manual on Fatigue Testing*, pp. 60-61, ASTM, Philadelphia, 1949.
16. A. Zarkades and F. R. Larson: "Properties of Textured Titanium Alloys," Metals and Ceramics Information Center Report, MCIC-74-20, July 1974.
17. P. G. Partridge: *Phil Mag.*, 1965, series 8, vol. 12, pp. 1043-54.
18. C. T. Beevers: *The Science, Technology and Application of Titanium*, pp. 535-45, Pergamon Press, Oxford, 1970.
19. A. Zarkades and F. R. Larson: Army Materials and Mechanics Research Center, AMMRC TN, 1973.
20. D. Eylon, C. M. Pierce, and J. A. Hall: "The Low Cycle Fatigue Behavior of IMI-685 Titanium Alloy," AFML, unpublished work.
21. D. Eylon, C. M. Pierce, and J. A. Hall: "The Correlation of Microstructure and Mechanical Properties in the Ti-11 Alloy at Room and Elevated Temperature," MATCON 74 Materials Science Symposium, Detroit, Mich., October 1974, abstract book, paper No. 150.
22. D. Shechtman and J. A. Robertson: "Localized Shear Related Fracture in the Ti-6Al-2Sn-4Zr-2Mo Alloy," Workshop on the Effect of Plastic Instability on the Fatigue and Fracture of Two-Phase Materials, Fairborn, Ohio, September 1974.